

## Theoretical Investigation of Ag(I) Acid-catalysed Cascade Benz Annulation of N-(3-(2-(4-Methoxybenzoyl)phenyl)prop-2-yn-1-yl)benzamide for Synthesis of Naphthooxazole

Nan Lu\*, Chengxia Miao and Xiaozheng Lan

College of Chemistry and Material Science, Shandong Agricultural University, Shandong Prov., P.R. China

\*Corresponding Author: Nan Lu, College of Chemistry and Material Science, Shandong Agricultural University, Shandong Prov., P.R. China.

DOI: 10.31080/ASPS.2023.07.0936

Received: January 25, 2023

Published: February 20, 2023

© All rights are reserved by Nan Lu, et al.

### Abstract

The mechanism is investigated for cascade benz annulation of N-(3-(2-(4-Methoxybenzoyl)phenyl)prop-2-yn-1-yl)benzamide catalyzed by Ag(I). The oxonium-ion generation and water nucleophilic addition induces ring opening hydroxylation, dual ketonization giving 1,5-diketone intermediate. Mediated by acid, the intramolecular cyclization, water elimination affords  $\beta$ -naphthol, from which the nucleophilic cyclization dehydration provides desired product naphthooxazole. The side reaction of acid-activated 5-exo-dig cyclization is accompanied by synergetic synchronous hydrolysis yielding indenone. The promotion of Ag(I) lies in the absolute energy and activation barrier decrease of oxonium-ion generation and water nucleophilic addition. The mediation of acid exists in intramolecular cyclization, nucleophilic cyclization dehydration and 5-exo-dig cyclization. The solvent influence of acid is smaller than Ag(I) from the reduction degree. These results are supported by Multiwfn analysis on FMO of specific TSs and MBO value of vital bonding, breaking.

**Keywords:** Oxazole-benzannulation; Naphtho[2,3-d]oxazole; Oxonium-Ion; 5-exo-dig; Cyclization Dehydration

### Introduction

As a family of heterocyclic compounds featuring benzene-fused oxazole ring structure, benzoxazole shows a broad range of medicinal properties and is frequently found in synthetic pharmaceuticals [1,2]. This core structure is also observed in many bioactive compounds isolated from a range of natural resources valuable for drug discovery and development [3-6]. To facilitate the production with a rapid and eco-friendly platform, various synthetic methods have been developed to prepare benzoxazole compounds. Besides the one-pot strategy for synthesis of 3-difluoromethyl benzoxazole-2-thiones in the presence of NaOt-Bu as a base using 2-aminophenol, sodium chlorodifluoroacetate, and elemental sulfur [7], enormous progress has been achieved

in transition-metal-catalyzed reactions. A highly enantioselective construction of hydroxyprolo-benzazoles was reported via copper-catalyzed dearomative [3+2] cycloaddition of benzazoles with donor-acceptor aminocyclopropanes [8]. The selective formal Pd/Cu-catalyzed C-H/C-H cross-coupling of azoles and (hetero)arenes was established through arylsulfonium intermediates producing a variety of 2-(hetero)aryl azoles [9]. The functionalization of bio-relevant heterocycles 2-arylbenzo[d]oxazole and 2-arylbenzo[d]thiazole was achieved through Ru(II)-catalyzed alkenylation with unactivated olefins [10].

The naphthoxazoles and fused heterobenzoxazoles can be prepared from 5-(aryl/furyl/thienyl/pyridyl ethenyl)oxazoles using Van Leusen reagent on irradiation in the presence of iodine

[11]. The dihydrobenzofuro[2,3-d]oxazole derivatives has been selectively constructed by means of base-controlled cyclization of multitasking N-phenoxyamides in two cascade reaction sequences [12]. A highly enantioselective alkyl and aryl/azolation can be achieved with the help of anionic tridentate ligands improving the reducibility of copper catalyst [13]. However, the synthesis of naphtho[2,3-d]oxazole employing 3-amino-2-naphthol derivatives as starting material is limited owing to the restriction of commercially available 3-amino-2-naphthol on naphthalene moiety [14]. The naphtho[2,3-d]oxazole could be functionalized at C-2 position of substrates using transition-metal catalysts such as palladium-catalyzed direct cyclopropylation of heterocycles, copper-catalyzed visible light-induced C-H arylation of benzoxazoles, and light-promoted enantioselective alkylation of azoles [15-17]. Alternatively, the desired product could also be obtained by delivering 2-aryl benzoxazoles through metal-free and redox-neutral De-CF<sub>3</sub> process [18]. To develop convenient construction of naphtho[2,3-d]oxazole analogues, challenges still exist in the invention of new synthetic methods utilizing versatile *ortho*-alkynylarylketone [19,20].

Among efficient ways leading to core structure [21,22], of special interest to us is the protocol of Ag(I) acid-catalyzed oxazole benz annulation for the synthesis of substituted naphthooxazole [23]. Although the silver catalyst was taken as the best activator for benz annulation of *ortho*-alkynylarylketones in previous methods [24,25], there is no report about detailed mechanistic study for this catalyzed Sonogashira coupling between *ortho*-iodoarylketone and N-propargylamide. Although a silver-catalyzed ketonization process is proposed followed by cyclization under acidic condition, the simple description is not sufficient especially the origin of by-product indenone. Will hydroxylation occur before ketonization during the process of nucleophilic addition with H<sub>2</sub>O of oxonium-ion intermediate? Is it possible for the cyclization of  $\beta$ -naphtholamide intermediate and following elimination to complete in one step of nucleophilic dehydration? As side reaction, why the hydrophilic cyclization of substrate containing quinoline moiety failed to generate naphthooxazole but indenone? To solve these mechanic problems in experiment, an in-depth theoretical study was necessary for this effective method especially the advantage of preparing various substituents on products in an unclear one-pot manner. The density functional theory (DFT) method was applied also focusing on the promotion of Ag(I) acid not mentioned in experiment at all.

## Methods

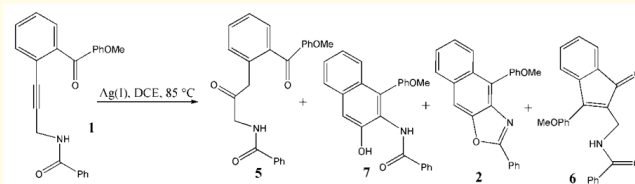
The geometry optimizations were performed at the B3LYP/BSI level with the Gaussian 09 package [26,27]. The mixed basis set of LanL2DZ for Ag and 6-31G(d) for nonmetal atoms [28-32] was denoted as BSI. Different singlet and multiplet states were clarified with B3LYP and ROB3LYP approaches including Becke's three-parameter hybrid functional combined with Lee-Yang-Parr correction for correlation [33,34]. The nature of each structure was verified by performing harmonic vibrational frequency calculations. Intrinsic reaction coordinate (IRC) calculations were examined to confirm the right connections among key transition-states and corresponding reactants and products. Harmonic frequency calculations were carried out at the B3LYP/BSI level to gain zero-point vibrational energy (ZPVE) and thermodynamic corrections at 358.15 K and 1 atm for each structure in dichloroethane (DCE). The solvation-corrected free energies were obtained at the M06-2X/6-311++G(d,p) (LanL2DZ for Ag) level in DCE by using integral equation formalism polarizable continuum model (IEFPCM) in Truhlar's "density" solvation model [35-39] on the B3LYP/BSI-optimized geometries.

As an efficient method obtaining bond and lone pair of a molecule from modern ab initio wave functions, NBO procedure was performed with Natural bond orbital (NBO3.1) to characterize electronic properties and bonding orbital interactions [40-42]. The wave function analysis was provided using Multiwfn\_3.7\_dev package [43] including composition of frontier molecular orbital (FMO) and Mayer bond order (MBO).

## Results and Discussion

Based on the experimental research previously [23-25], the mechanism was explored for Ag(I) acid-catalyzed cascade oxazole-benzannulation of N-(3-(2-(4-Methoxybenzoyl)phenyl)prop-2-yn-1-yl)benzamide 1 leading to 1,5-diketone 5,  $\beta$ -naphthol 7, desired product naphthooxazole 2, and side product indenone 6 (Scheme 1). As illustrated by Scheme 2, the major reaction contains: (1) Ag(I)-catalyzed oxonium-ion i1 generation and its nucleophilic addition with H<sub>2</sub>O inducing ring opening hydroxylation, (2) dual ketonization of dihydroxy complex i4 giving 1,5-diketone intermediate 5, (3) stepwise intramolecular cyclization of protonated 5 affording i6, elimination of H<sub>2</sub>O giving 7, concerted nucleophilic dehydration-cyclization of protonated 7 providing i8, and dehydroaromatization forming 2. The optimized structures

of TSs and intermediates in scheme 2 are listed by figure 1 and Supplementary Figure S1, respectively. Table 1 and Supplementary Table S1 show the activation energy of all reactions and the relative energies of all stationary points. The Gibbs free energies in DCE solution phase are discussed here to be in accordance with experiment.



**Scheme 1:** Ag(I) acid-catalyzed cascade oxazole benz annulation of N-(3-(2-(4-Methoxybenzoyl)phenyl)prop-2-yn-1-yl)benzamide 1 leading to 1,5-diketone 5, β-naphthol 7, product naphthooxazole 2, and side product indenone 6.

**Scheme 2:** Proposed reaction mechanism of Ag(I) acid-catalyzed cascade oxazole benz annulation of 1 yielding 5, 7, 2. TS is named according to the two intermediates it connects.

**Figure 1:** Optimized structure of transition states for Ag(I) acid-catalyzed cascade oxazole-benzannulation of 1 (Bond lengths in nm).

TS	$\Delta G_{\text{gas}}^{\ddagger}$	$\Delta G_{\text{sol}}^{\ddagger}$
ts-i01	25.2	16.2
ts-i23	12.1	13.2
ts-i24	59.5	55.7
ts-i34	5.7	8.1
ts-i5-01	3.2	3.2
ts-i5	62.6	62.5
ts5h6	2.4	2.4
ts67h	30.5	30.9
ts7h8	58.5	57.5
ts-i910	31.2	35.8
ts-i11-01	31.9	34.5
ts-i11-02	25.8	28.2
ts-i11-21	41.8	35.9
ts-i11-13	12.5	14.8

**Table 1:** The activation energy (in  $\text{kJ mol}^{-1}$ ) of all reactions in gas and solvent.

Species	$\Delta G_{\text{gas}}$	$\Delta G_{\text{sol}}$	$\Delta \Delta G_{\text{sol-gas}}$
1+ag			
i0	0.0	0.0	-58.9
ts-i01	25.2	16.2	-67.9
i1	-0.5	-2.7	-61.1
1+ag+h2o			
i2	0.0	0.0	-60.5
ts-i23	12.1	13.2	-59.4
ts-i24	59.5	55.7	-64.4
i3	6.9	5.7	-61.7
ts-i34	12.6	13.8	-59.4
i4	5.7	6.6	-59.6
1+h2o			
i5-0	0.0	0.0	-24.3
ts-i5-01	3.2	3.2	-24.3
i5-1	-47.4	-47.8	-24.7
ts-i5	15.3	14.7	-24.8
5	-60.3	-58.3	-22.2

**Figure S1:** Optimized structures of substrates, catalysts, and intermediates proposed in Scheme 2 and Scheme 3. (Bond lengths in nm).

1+h2o+h			
5h+	0.0	0.0	-58.8
ts5h6	2.4	2.4	-58.8
i6	-2.1	-2.5	-59.2
ts67h	28.4	28.4	-58.9
7h+h2o	-20.1	-17.3	-55.9
1			
7	-52.7	-50.2	-22.9
1+h			
7h+	0.0	0.0	-56.3
ts7h8	58.5	57.5	-57.2
i8	-1.6	-0.3	-54.9
1-h2o			
2	-42.4	-41.3	-19.1
1+h			
i9	0.0	0.0	-63.5
ts-i910	31.2	35.8	-59.0
i10	-8.0	-3.8	-59.3
1+h2o+h			
i11-0	0.0	0.0	-60.0
ts-i11-01	31.9	34.5	-57.4
ts-i11-02	25.8	28.2	-57.6
i11-2	-41.6	-38.6	-56.9
ts-i11-21	0.2	-2.7	-62.8
i11-1	-31.5	-32.0	-60.5
ts-i11-13	-18.9	-17.2	-58.2
i11-3	-38.1	-33.6	-55.5
1			
6	-40.7	-33.7	-18.3

**Table S1:** Calculated relative energies (all in  $\text{kJ mol}^{-1}$ , relative to isolated species) for the ZPE-corrected Gibbs free energies ( $\Delta G_{\text{gas}}^{\ddagger}$ ), Gibbs free energies for all species in solution phase ( $\Delta G_{\text{sol}}^{\ddagger}$ ) at 358 K by M06-2X/6-311++G(d,p)//B3LYP/6-31G(d) method and difference between absolute energy.

TS	Energy level (global barrier)		Activation energy (local barrier)	
	$\Delta G_{\text{gas}}^{\ddagger}$	$\Delta G_{\text{sol}}^{\ddagger}$	$\Delta G_{\text{gas}}^{\ddagger}$	$\Delta G_{\text{sol}}^{\ddagger}$
ts-i01 (120i)	25.2	16.2	25.2	16.2
ts-i23 (418i)	12.1	13.2	12.1	13.2

ts-i24 (1479i)	59.5	55.7	59.5	55.7
ts-i34 (198i)	12.6	13.8	5.7	8.1
ts-i5-01 (82i)	3.2	3.2	3.2	3.2
ts-i5 (2182i)	15.3	14.7	62.6	62.5
ts5h6 (290i)	2.4	2.4	2.4	2.4
ts67h (1465i)	28.4	28.4	30.5	30.9
ts7h8 (1532i)	58.5	57.5	58.5	57.5
ts-i910 (383i)	31.2	35.8	31.2	35.8
ts-i11-01 (359i)	31.9	34.5	31.9	34.5
ts-i11-02 (313i)	25.8	28.2	25.8	28.2
ts-i11-21 (534i)	0.2	-2.7	41.8	35.9
ts-i11-13 (220i)	-18.9	-17.2	12.5	14.8

**Table S2:** The energy level and the activation energy (in  $\text{kJ mol}^{-1}$ ) of all reactions in the gas, solution phase calculated with M06-2X/6-311++G(d,p)//B3LYP/6-31G(d) method.

### Ag(I)-catalyzed oxonium-ion generation and H<sub>2</sub>O nucleophilic addition

Illustrated by black dash line of figure 2a, the oxonium-ion intermediate i1 is generated via ts-i01 from the reaction between 1 and silver catalyst Ag(I) with the activation energy barrier of  $16.2 \text{ kJ mol}^{-1}$  relative to an initial complex i0. The transition vector corresponds to remarkable bonding of C1–O1 (0.24 nm), C2–Ag (0.24 nm) and elongation of C1–C2 triple bond to double (0.12 nm) (Supplementary Figure S2a). This step is calculated to be exergonic by  $-2.7 \text{ kJ mol}^{-1}$ . In the structure of i1, a six membered ring is formed with C1–C2, C1–O1 bonds (0.14, 0.14 nm) and the positive charge is transferred to O1. The following nucleophilic addition of H<sub>2</sub>O is facilitated under the catalysis of Ag, which is completely linked to alkyne C2 (0.21 nm). FMO calculations were applied for typical TSs to get more qualitative evidence of structural analysis [28-32]. The visual orbitals of Highest Occupied Molecular Orbital (HOMO) and Lowest Unoccupied Molecular Orbital (LUMO) were analyzed (Figure 3) together with MBO results for the orbital contribution of bonding atoms (Table 2 and Table 3). HOMO of ts-i01 is mainly on O1 (7.05%), minor on C2 (0.09%) and LUMO greatly on C1, Ag (7.87%, 83.61%). This distribution favors the

concerted nucleophilic attack from O1, C2 to C1, Ag, respectively. What's more, MBO values of O1...C1, C2...Ag (0.118, 0.435) echoes the formation of O1-C1, C2-Ag bond as well as the stretching of C1-C2 (2.136).

**Figure 2:** Relative Gibbs free energy profile in solvent phase starting from complex (a) i0 and i2, (b) i5-0, (c) 5h+ and 7h+, (d) i9 and i11-0.

**Figure S2:** Evolution of bond lengths along the IRC for (a) ts-i01 (b) ts-i23 (c) ts-i34 (d) ts-i5 (e) ts5h6 (f) ts67h (g) ts7h8 (h) ts-i910 (i) ts-i11-01 (j) ts-i11-13 at the M06-2X/6-311++G(d,p) level.

**Figure 3:** Highest Occupied Molecular Orbital (HOMO) and Lowest Unoccupied Molecular Orbital (LUMO) of typical transition states ts-i01, ts-i23, ts-i34, ts67h, ts7h8, and ts-i11-01. Different colors are used to identify the phase of the wave functions.

	O1	C1	C2	Ag	
ts-i01 HOMO	7.05	0.12	0.09	0.03	
ts-i01 LUMO	1.58	7.87	1.78	83.61	
	C5	O3	H1	O2	
ts-i23 HOMO	0.82	0.13	0.01	0.05	
ts-i23 LUMO	0.01	0.01	0	0.09	
	C5	O1	H1	O2	
ts-i34 HOMO	0.32	8.62	0.05	0.11	
ts-i34 LUMO	0.11	0.79	0.17	0.15	
	C5	O3	C6	H5	
ts67h HOMO	0.87	0.02	1.18	0.02	

ts67h LUMO	2.69	2.71	7.14	11.30	
	C7	O1	H4	O2	
ts7h8 HOMO	0.20	0.17	0.01	0.14	
ts7h8 LUMO	2.61	0.58	0.84	0.48	
	C5	C1	C2	O3	H2
ts-i11-01 HOMO	0.86	7.53	5.98	2.73	0.05
ts-i11-01 LUMO	31.78	1.41	24.41	3.36	0.94

**Table 2:** Contribution (%) of Natural Atomic Orbital (NAO) to Highest Occupied Molecular Orbital (HOMO), and Lowest Unoccupied Molecular Orbital (LUMO) of typical TSs.

	O1...C1	C1...C2	C2...Ag	
ts-i01	0.118	2.136	0.435	
	C5...O3	O3...H1	H1...O2	
ts-i23	0.580	0.386	0.295	
	C5...O1	O2...H1	H1...O1	
ts-i34	0.436	0.270	0.440	
	C5...O3	C6...H5	H5...O3	
ts67h	0.784	0.402	0.287	
	C7...O1	O1...H4	H4...O2	C7...O2
ts7h8	0.767	0.358	0.332	0.742
	C5...C1	C2...O3	O3...H2	
ts-i11-01	0.398	0.216	0.716	

**Table 3:** Mayer bond order (MBO) of typical TSs.

As the starting point of relative Gibbs free energy profile (red dash line of Figure 2a), the energy of i2 binding i1 and one water molecule is set as 0.0 kJ mol<sup>-1</sup>, from which the nucleophilic attack of H<sub>2</sub>O takes place in step 1 via ts-i23 to achieve the simultaneous bonding in the form of O3H2 to C5 and hydrogen atom H1 to O2. The transition vector of ts-i23 is about the closing of O3 to C5 and departure of H1 from O3 to O2 (0.16, 0.11, 0.13 nm) (Figure S2b). Thus, the preliminary dual hydroxylation is accomplished on C5 and C7 in intermediate i3 also involving O2H1...O1 H bond (0.16 nm). The activation energy barrier is 13.2 kJ mol<sup>-1</sup> with respect

to i2. Benefited from this, the barrier of step 2 is decreased to be 8.1 kJ mol<sup>-1</sup> via ts-i34, the transition vector of which indicates a concerted process of proton transfer and ring opening. That is the leaving of H1 from O2 to O1 and cleavage of C5-O1 bond (0.14, 0.11, 0.18 nm) (Figure S2c) making the final dual hydroxylation shifting to be on C5 and C1 in resultant i4 slightly endothermic by 6.6 kJ mol<sup>-1</sup>. Thereby step 1 is determined to be rate-limiting of this stepwise nucleophilic addition with H<sub>2</sub>O kinetically. As an alternative possible path (blue dash line of Figure 2a), ts-i24 was located between i2 and i4 corresponding to the direct ring opening under the nucleophilic attack by H<sub>2</sub>O and protonation of O1 by the same H<sub>2</sub>O meanwhile. However, the activation energy barrier is high to be 55.7 kJ mol<sup>-1</sup> denoting impossibility. The reaction should be stopped at this step. Hence, the nucleophilic addition with H<sub>2</sub>O via one step is excluded compared with stepwise mode.

The correctness of ts-i23 and ts-i34 is also verified by FMO analysis. For ts-i23, HOMO and LUMO on C5 and O2 (0.82%, 0.09%) allows to be attacked by nucleophile water and to receive proton. The accompanied bonding can be demonstrated by MBO values of C5...O3, O3...H1 and H1...O2 (0.580, 0.386, 0.295). HOMO of ts-i34 is on O1 and C5 (8.62%, 0.32%). There is an even distribution of LUMO on C5, O1, H1, O2 (0.11%, 0.79%, 0.17%, 0.15%). MBO value of C5...O1 (0.436) suggests the ongoing ring opening.

### Dual ketonization

After the release of Ag(I), the 1,5-dihydroxyl intermediate i4 would isomerize to 1,5-diketone intermediate 5, which is also a stable product obtained in experiment. Two steps are required to achieve this dual ketonization. Shown by the relative Gibbs free energy profile (Figure 2b), the starting point i5-0 is a neutral 1,5-dihydroxyl complex without Ag(I), from which the hydroxyl H2 on C5 shifts to the middle C2 in step 1 via ts-i5-01, the transition vector of which corresponds to breaking of O3-H2 bond (0.10 nm) and linking of H2-C2 (0.16 nm). The first ketonization is achieved with a small activation energy barrier of 3.2 kJ mol<sup>-1</sup> leading to i5-1, a structure rather stable with the exergonic energy high to be -47.8 kJ mol<sup>-1</sup>. It is thus clear that this step is fairly easy both kinetically and thermodynamically owing to the active intermediate carbon of accumulated diene. Contrast with this, the second ketonization seems to be a little difficult via ts-i5 in step 2 affording the final desired 5 continuously releasing heat by -58.3 kJ mol<sup>-1</sup>. Although

the activation energy is somewhat high with respect to i5-1, the relative energy level of ts-i5 is  $14.7 \text{ kJ mol}^{-1}$ . Especially the correctness is strictly verified by the vibration vector about the transferring of H1 from hydroxyl on C1 to C2 (0.13, 0.15 nm) (Figure S2d). Hence, the second ketonization is rate-limiting step for the dual ketonization process.

### Intramolecular cyclization, elimination of H<sub>2</sub>O, and nucleophilic cyclization dehydration

Under acidic conditions, the ketone group on C5 of intermediate 5 is protonated by H<sup>+</sup> and at the same time another ketone group on C1 receives H atom on adjacent C6 becoming its enol isomer. Characterized by positive O3H3 and neutral O1H4, the optimized structure 5h<sup>+</sup> is taken as the starting point of relative Gibbs free energy profile (black dash line of Figure 2c). The intramolecular cyclization of enol nucleophiles takes place in step 1 via ts5h6 with low activation energy of  $2.4 \text{ kJ mol}^{-1}$  providing stable intermediate i6 exothermic by  $-2.5 \text{ kJ mol}^{-1}$ . The transition vector is simple to be the nucleophilic attack of C6 to positive C5 (0.20 nm) (Figure S2e). Once the new six-membered ring is cyclized with bonding C5-C6, the positive charge is shifted to O1H4 in i6, from which step 2 occurs via ts67h with activation energy of  $30.9 \text{ kJ mol}^{-1}$  continuously releasing heat by  $-17.3 \text{ kJ mol}^{-1}$ . The transition vector concerns the breaking of C5-O3 and the leaving of H5 from C6 to O3 (0.15, 0.14, 0.13 nm) to realize the elimination of water molecule H5-O3H3 (Figure S2f). The neutral product  $\beta$ -naphtholamide 7 is provided after elimination of water and dehydroaromatization. The positive charge is taken away along with the leaving of H1 on C2 making the structure of 7 rather stable with the relative energy of  $-50.2 \text{ kJ mol}^{-1}$ .

To model the next nucleophilic cyclization dehydration, another protonated structure 7h<sup>+</sup> was located as the starting point of relative Gibbs free energy profile (red dash line of Figure 2c) by adding an extra H6 to enolize O2 under acidic condition. This process is determined to be concerted nucleophilic cyclization and elimination via ts7h8 with high activation energy of  $57.5 \text{ kJ mol}^{-1}$  affording positively charged oxazole intermediate i8 ( $-0.3 \text{ kJ mol}^{-1}$ ), which transforms to final naphtho[2,3-d]oxazole 2 much more stable ( $-41.3 \text{ kJ mol}^{-1}$ ) without water and proton. Despite the barrier is somewhat high, the rate constant  $k$  is calculated to be about  $5.6 \times 10^{-23} \text{ s}^{-1}$  applying the experimental temperature

(85 °C) together with the exothermic energy. Thereby, the value with B3LYP/6-311++G(d,p) method indicates that the last step is difficult in concerted mode only possible at high temperature. Fortunately, the structure of ts7h8 connecting 7h<sup>+</sup> and i8 can be ensured through its transition vector containing the closing of O1-C7, breaking of C7-O2 bond, transferring of H4 from O1 to O2 (0.15, 0.15, 0.12, 0.13 nm) (Figure S2g). In order to obtain the ideal product, the high temperature condition in experiment is necessary, which also makes other by-products easy to yield especially the indenone 6.

FMO analysis was also applied to confirm a series of processes indicated by the vibration mode of ts67h and ts7h8. HOMO of ts67h is distributed main on C5, C6 (0.87%, 1.18%) and LUMO on H5, O3 (11.30%, 2.71%) are ready for the departure of H5-O3H3 from six-membered ring. What's more, MBO values of C5...O3, C6...H5 and H5...O3 (0.784, 0.402, 0.287) agrees well with the cleavage of C5-O3, C6-H5 and connection of H5-O3. For ts7h8, HOMO on O1, C7 (8.62%, 0.32%) facilitates the attachment of C7...O1 in accordance with the MBO value (0.767). The synchronous fracture of O2 from C7 and H4 from O1 can be validated by LUMO on C7, O2, H4, O1 (2.61%, 0.48%, 0.84%, 0.58%) as well as MBO values of C7...O2 and O1...H4 (0.742, 0.358).

### Acid-activated 5-exo-dig cyclization, hydrolysis

In experiment, the substrate 1 containing quinoline moiety failed to generate desired 2 but indenone 6. The mechanism was researched for acid-activated 5-exo-dig cyclization, hydrolysis of 1 in the absence of Ag(I) by adding one H<sup>+</sup> and H<sub>2</sub>O (solid arrow of Scheme 3). In this case, the cyclization catalyzed by acid is accompanied by synergetic synchronous hydrolysis. An intermediate indenediol i11-1 is obtained via the link of water molecule to positive middle alkyne carbon and negative heteroatom in forms of hydroxyl and hydrogen, respectively. Next, the hydrogen is given by heteroatom together with one hydroxyl removing as water and another hydroxyl loses its proton to form indenone 6.

The pure cyclization was taken into account by modeling the system only with an extra H<sup>+</sup> (dash arrow of Scheme 3). With O1H1, the complex is located as starting point i9, from which the electrophilic attack of alkene-to-alkyne proceeds via ts-i910 with activation energy of  $35.8 \text{ kJ mol}^{-1}$  resulting in indenol i10 (black

**Scheme 3:** Proposed mechanism for the acid-activated 5-exo-dig cyclization, hydrolysis of 1 yielding 6. TS is named according to the two intermediates it connects.

dash line of Figure 2d). The transition vector displays prominent approaching of relatively positive C5 (0.078) to C1 (0.039) and C2 (0.061) closing to carbon on benzene ring (-0.265) with high electron density (0.20, 0.24 nm). The structure of i10 is unfavorable in thermodynamics owing to the positive alkyne C2 must be bonded to other atoms.

In this case, the synchronous hydrolysis is expected to be more favorable paths (red and blue dash line of Figure 2d) especially considering the large amount of water. The red one illustrates the extra H<sub>2</sub>O links to C2 with hydroxyl O3H3 and the relatively negative heteroatom N with H2 concurrent with cyclization via ts-i11-01 in a concerted mode. The transition vector manifests closing of C5 to C1 and C2 to O3 (0.21, 0.21 nm) as well as cooperative H2 leaving from O3 to N (0.10, 0.23 nm) (Figure S2i). With respect to i11-0, the activation energy of this step 1 in concerted path is 34.5 kJ mol<sup>-1</sup> exothermic by -32.0 kJ mol<sup>-1</sup> leading to i11-1, which is remarkably superior over i10 (-3.8 kJ mol<sup>-1</sup>). Two H bonds

N-H2...O1 and N-H2...O2 (0.18, 0.24 nm) exist effectively stabilizing the structure of i11-1. Alternatively, the stepwise H transfer could not be excluded, that is H2 transfer to O2 and then to N as shown by the blue one. Step 1 of stepwise path occurs via ts-i11-02 with decreased barrier of 28.2 kJ mol<sup>-1</sup> and increased exothermic energy of -38.6 kJ mol<sup>-1</sup> giving i11-2, from which step 2 takes place via ts-i11-21 with a barrier of 35.9 kJ mol<sup>-1</sup>. Thereby, step1 seems to be more favorable than that of step 1 in concerted mode both from kinetics and thermodynamics. While there is no much distinction compared with rate-limiting step 2. The rationality of ts-i11-01 is consistent with its FMO result. LUMO main on C5, C2 (31.78%, 24.41%), minor on C1, O3, H2 (1.41%, 3.36%, 0.94%) and HOMO evenly distributed on C1, O3, N (7.53%, 2.73%, 0.28%) are conducive to cyclization and simultaneous resolution of water molecule, which also can be confirmed by MBO values of C5...C1 and C2...O3 (0.398, 0.216).

From indenediol i11-1, the dehydration proceeds via ts-i11-13 concretely through hydroxyl O1H1 breaking off from C5 forming one H<sub>2</sub>O with H2 given by N. The transition vector contains cleavage of C5-O1, N-H2 and connection of O1-H2 (0.19, 0.19, 0.1 nm) (Figure S2j). The deprotonation of another hydroxyl O3H3 makes it carbonyl yielding final side product indenone 6 exothermic by -33.7 kJ mol<sup>-1</sup>. The last step is readily accessible owing to a low activation energy barrier of 14.8 kJ mol<sup>-1</sup>.

### Solvent effect

In view of the solvent effect on reaction with ions estimated by our approach [28-32], it's expected to have great impact on this charged system catalyzed by Ag(I) acid. The difference value of absolute energies between in gas phase and DCE solution are listed for all stationary points (Table S1). Generally, as the normal solvent effect from kinetics, the absolute energies in solution should be lower than those in gas phase. The larger the reduction value, the more readily the path. From i0 to i4, initial two processes of oxonium-ion generation and H<sub>2</sub>O nucleophilic addition both catalyzed by Ag(I) present the largest decreased degree of -59~-65 kcal mol<sup>-1</sup>. In the case of only mediated by acid without the participation of Ag(I), the reduction extent is downhill slightly (-55~-60 kcal mol<sup>-1</sup>) for intramolecular cyclization, elimination of H<sub>2</sub>O from 5h+ to 7h+h2o, nucleophilic cyclization dehydration from 7h+ to i8 and 5-exo-dig cyclization, hydrolysis from i11-0 to i11-3.

The minimum reduction value  $-22\sim-24$  kcal mol<sup>-1</sup> appears when there is no Ag(I) catalyst or acid for dual ketonization from 5 to 6. For four kinds of neutral structure obtained by experiment, the reduced degree of intermediate 1,5-diketone 5,  $\beta$ -naphthol 7 ( $-22$  kJ mol<sup>-1</sup>) is slightly larger than that of product 2, side product indenone 6 ( $-19$  kJ mol<sup>-1</sup>). Accordingly, the promotion by Ag(I) produced the most favorable influence of solvation on this cascade oxazole benz annulation, followed by acid from a kinetic point of view.

## Conclusion

Our DFT calculations provide the first theoretical investigation on cascade oxazole-benzannulation of N-(3-(2-(4-Methoxybenzoyl)phenyl)prop-2-yn-1-yl)benzamide catalyzed by Ag(I). The generation of oxonium-ion and its nucleophilic addition with water induces ring opening hydroxylation, dual ketonization giving 1,5-diketone intermediate. Mediated by acid, the intramolecular cyclization, elimination of water affords  $\beta$ -naphthol, from which the nucleophilic cyclization dehydration provides desired naphthooxazole. The side reaction of acid-activated 5-exo-dig cyclization is accompanied by synergetic synchronous hydrolysis yielding indenone. An intermediate indenediol is obtained via the link of water to positive alkyne carbon and negative heteroatom in forms of hydroxyl and hydrogen. Then the hydrogen given by heteroatom together with one hydroxyl removes as water.

The decreased absolute energies in solution compared with in gas suggest a favorable solvation effect kinetically. The promotion of Ag(I) lies in the barrier decrease of oxonium-ion generation and water nucleophilic addition. The mediation of acid exists in intramolecular cyclization, nucleophilic cyclization dehydration and 5-exo-dig cyclization, which exerts smaller solvent influence than Ag(I) from the reduction degree. These results are supported by Multiwfn analysis on FMO of specific TSs and MBO value of vital bonding, breaking.

## Acknowledgements

This work was supported by National Natural Science Foundation of China (21973056, 21972079) and Natural Science Foundation of Shandong Province (ZR2019MB050).

## Bibliography

1. Lamb YN., *et al.* "Tafamidis: a review in transthyretin amyloidosis with polyneuropathy". *Drugs* 79.8 (2019): 863-874.
2. Singh S., *et al.* "Recent Advances in the Development of Pharmacologically Active Compounds That Contain a Benzoxazole Scaffold". *The Asian Journal of Organic Chemistry* 4.2 (2015): 1338-1361.
3. Jiao WH., *et al.* "Cinerols, Nitrogenous Meroterpenoids from the Marine Sponge *Dysidea cinerea*". *The Journal of Natural Products* 82.9 (2019): 2586-2593.
4. Sasmal S., *et al.* "A First Synthesis of Bis (Benzoxazole) Natural Products: Nataxazole and AJI9561 via Benzoxazole C-H Activation". *Synthesis* 47.3 (2015): 711-3716.
5. Pal S., *et al.* "Benzoxazole Alkaloids: Occurrence, Chemistry, and Biology". *Alkaloids Chemistry and Biology* 79 (2018): 71-137.
6. Ouyang H., *et al.* "An E. coli-Based Biosynthetic Platform Expands the Structural Diversity of Natural Benzoxazoles". *ACS Synthetic Biology* 10.9 (2021): 2151-2158.
7. Li Z., *et al.* "One-Pot Synthesis of 3-Difluoromethyl Benzoxazole-2-thiones". *Organic Letter* 20.20 (2018): 6407-6410.
8. Zhang MC., *et al.* "Cu-catalyzed Asymmetric Dearomatic [3 + 2] Cyclo-addition Reaction of Benzazoles with Aminocyclopropanes". *Chemistry* 5.1 (2019): 156-167.
9. Tian ZY., *et al.* "Pd/Cu-Catalyzed C-H/C-H Cross Coupling of (Hetero)Arenes with Azoles through Arylsulfonium Intermediates". *Organic Letter* 23.11 (2021): 4400-4405.
10. Pipaliya BV., *et al.* "Ruthenium (II) Catalyzed C (sp<sup>2</sup>)-H Bond Alkenylation of 2-Arylbenzo [d] oxazole and 2-Arylbenzo [d] thiazole with Unactivated Olefins". *Chemistry Asian Journal* 16.1 (2021): 87-96.
11. Sagud I., *et al.* "Photochemical Approach to Naphthoxazoles and Fused Heterobenzoxazoles from 5- (Phenyl/heteroarylethenyl)oxazoles". *Organic Chemistry* 76.8 (2011): 2904-2908.
12. Li M., *et al.* "N-Phenoxyamides as Multitasking Reagents: Base-Controlled Selective Construction of Benzofurans or Dihydrobenzofuro[2,3-d]oxazoles". *The Journal of Organic Chemistry* 84.13 (2019): 8523-8530.

13. Ma X., *et al.* "Asymmetric Alkyl and Aryl/Azolation of Alkenes via a Single Cu (I) Complex". *ACS Catalyst* 11.9 (2021): 5108-5118.
14. Zhang J., *et al.* "Thiol substrate-promoted dehydrogenative cyclization of arylmethyl thiols with ortho-substituted amines: a universal approach to heteroaromatic compounds". *Organic Chemistry Frontiers Journal* 6.13 (2019): 2844-2849.
15. Wu X., *et al.* "Palladium-Catalyzed Direct Cyclopropylation of Hetero-cycles". *Angewandte Chemie International Edition* 54.33 (2015): 9601-9605.
16. Ma X., *et al.* "Visible Light-Induced Copper-Catalyzed C-H Arylation of Benzoxazoles". *Chinese Journal of Chemistry* 38.11 (2020): 1299-1303.
17. Li C., *et al.* "Light-Promoted Copper-Catalyzed Enantioselective Alkylation of Azoles". *Angewandte Chemie International Edition* 60.4 (2021): 2130-2134.
18. Qiao X., *et al.* "Delivering 2-Aryl Benzoxazoles through Metal-Free and Redox-Neutral De-CF<sub>3</sub> Process". *The Journal of Organic Chemistry* 86.19 (2021): 13548-13558.
19. Thongsornkleeb C., *et al.* "Utilization of ortho-alkynylarylcarbonyl derivatives for creating structurally diverse chemical compounds". *Organic and Biomolecular Chemistry* 19.27 (2021): 5982-5998.
20. Pradhan TR., *et al.* "An Overview of Water-Mediated Alkyne Functionalization by Neighboring Group Participation of Carbonyl Groups". *Advanced Synthesis and Catalysis* 362.22 (2020): 4833-4860.
21. Jaithum K., *et al.* "Diastereoselective Synthesis of Spirocyclic Ether from ortho-Carbonylarylacetylenols via Silver-Catalyzed Cyclization under Acidic Conditions". *Advanced Synthesis and Catalysis* 363.15 (2021): 3812-3834.
22. Laohapaisan P., *et al.* "Ag (I)-Catalyzed/Acid-Mediated Cascade Cyclization of ortho-Alkynylaryl-1, 3-dicarbonyls to Access Arylnaphthalenelactones and Furanonaphthol Libraries via Aryl-Disengagement". *Chemistry - Asian Journal* 17.1 (2022): e202101212-1-e202101212-15.
23. Rodphon W., *et al.* "Synthesis of Naphtho[2,3-d]oxazoles via Ag (I) Acid-Mediated Oxazole-Benzannulation of ortho-Alkynylamidoarylketones". *The Journal of Organic Chemistry* (2020).
24. Álvarez-Corral M., *et al.* "Silver-mediated synthesis of heterocycles". *Chemical Review* 108.8 (2008): 3174-3198.
25. Fang G., *et al.* "Silver-catalysed reactions of alkynes: recent advances". *Chemical Society Reviews* 44.22 (2015): 8124-8173.
26. Frisch MJ., *et al.* Gaussian 09, Revision B.01, Gaussian, Inc, Wallingford, CT (2009).
27. Hay PJ., *et al.* "Ab initio effective core potentials for molecular calculations-potentials for the transition-metal atoms Sc to Hg". *The Journal of Chemical Physics* 82.1 (1985): 270-283.
28. Lv H., *et al.* "Ionic Liquid Catalyzed C-C Bond Formation for the Synthesis of Poly substituted Olefins". *European Journal of Organic Chemistry* 2022.45 (2022): e202201222 .
29. Zhuang H., *et al.* "Bu<sub>4</sub>NHSO<sub>4</sub>-Catalyzed Direct N-Allylation of Pyrazole and its Derivatives with Allylic Alcohols in Water: A Metal-free, Recyclable and Sustainable System". *Advanced Synthesis and Catalysis* 363.24 (2021): 5461-5472.
30. Lu N., *et al.* "Theoretical investigation on transformation of Cr (II) to Cr (V) complexes bearing tetra-NHC and group transfer reactivity". *International Journal of Quantum Chemistry* 120 (2020): e26340.
31. Lu N., *et al.* "Theoretical investigation on the mechanism and enantioselectivity of organocatalytic asymmetric Povarov reactions of anilines and aldehydes". *International Journal of Quantum Chemistry* 120 (2020): e26574.
32. Frenking G., *et al.* "The Nature of the Bonding in Transition-Metal Compounds". *Chemical Review* 100.2 (2000): 717-774.
33. Becke AD. "Density-functional thermochemistry. IV. A new dynamical correlation functional and implications for exact-exchange mixing". *The Journal of Chemical Physics* 104.3 (1996): 1040-1046.
34. Lee CT., *et al.* "Development of the Colle-Salvetti correlation-energy formula into a functional of the electron density". *Physical Review B* 37.2 (1988): 785-789.
35. Tapia O. "Solvent effect theories: Quantum and classical formalisms and their applications in chemistry and biochemistry". *Journal of Mathematical Chemistry* 10.1 (1992): 139-181.
36. Tomasi J., *et al.* "Molecular Interactions in Solution: An Overview of Methods Based on Continuous Distributions of the Solvent". *Chemical Review* 94.7 (1994): 2027-2094.
37. Simkin BY., *et al.* "Quantum Chemical and Statistical Theory of Solutions—A Computational Approach". Ellis Horwood, London (1995).

38. Tomasi J., *et al.* "Quantum Mechanical Continuum Solvation Models". *Chemical Review* 105.8 (2005): 2999-3093.
39. Marenich AV., *et al.* "Universal solvation model based on solute electron density and on a continuum model of the solvent defined by the bulk dielectric constant and atomic surface tensions". *The Journal of Physical Chemistry B* 113.18 (2009): 6378-6396.
40. Reed AE., *et al.* "Natural population analysis". *The Journal of Chemical Physics* 83.2 (1985): 735-746.
41. Reed AE., *et al.* "Intermolecular interactions from a natural bond orbital donor-acceptor view point". *Chemical Review* 88.6 (1988): 899-926.
42. Foresman, JB., *et al.* "Exploring Chemistry with Electronic Structure Methods". 2<sup>nd</sup> ed., Gaussian, Inc., Pittsburgh (1996).
43. Lu T., *et al.* "Multiwfn: A multifunctional wavefunction analyzer". *Journal of Computational Chemistry* 33.5 (2012): 580-592.